oxide libraries with sites of 200 μm by 200 μm and spacings of 50 μm between sites.

Because this approach differs from conventional bulk synthesis and thin film fabrication methods, standard synthetic conditions may require modification in some instances. For example, synthesis of the $YBa_2Cu_3O_{7-x}$ superconductor (*11*) from a film generated by sequential deposition of BaF_2, Y_2O_3, and CuO in a 1:2:3 molar ratio (~400 Å of CuO) required low-temperature annealing of samples (200 to 400°C) before high-temperature sintering (840°C). Diffusion processes at low temperatures may facilitate formation of a homogeneous intermediate without nucleation of stable lower-order phases (*12*). We used this protocol to reproducibly synthesize $YBa_2Cu_3O_{7-x}$ superconducting films of sizes as small as 200 μm by 200 μm with metallic behavior and a T_c of ~90 K (Fig. 2D). A 128-member library derived from $BaCO_3$, Y_2O_3, Bi_2O_3, CaO, $SrCO_3$, and CuO was then generated to determine the compatibility of different families of copper oxide superconductors with a common processing condition. After annealing and high-temperature sintering (840°C), sites containing $BiSrCaCuO_x$ and $YBa_2Cu_3O_x$ were found to be superconducting.

The work described above effectively extends the combinatorial approach from biological and organic molecules to the remainder of the periodic table. Improved synthetic methodology may allow the parallel synthesis of larger libraries by means of higher-resolution physical masks or photolithography. Moreover, high-resolution scanning (susceptibility and Eddy current) detectors, as well as multichannel contact probes using spring-loaded contact pins, are being developed to facilitate library analysis. Nonetheless, the methodology, even in its current form, has already shown its effectiveness as a tool for discovering new materials. For example, new giant magnetoresistive oxides (*14*) containing cobalt have been found in libraries of Ln-M-X oxides, where Ln = La or Y, M = Ba, Sr, Ca, or Pb, and X = Mn or Co (*15*).

REFERENCES AND NOTES

1. *Materials Science and Engineering in the 1990s* (National Academy Press, Washington, DC, 1989).
2. F. J. DiSalvo, *Science* **247**, 649 (1990).
3. A. Nisonoff, J. E. Hopper, S. B. Spring, *The Antibody Molecule* (Academic Press, New York, 1975).
4. S. J. Pollack, J. W. Jacobs, P. G. Schultz, *Science* **234**, 1570 (1986); A. Tramontano, K. D. Janda, R. A. Lerner, *ibid.*, p. 1566; R. A. Lerner, S. J. Benkovic, P. G. Schultz, *ibid.* **252**, 659 (1991).
5. J. K. Scott and G. P. Smith, *ibid.* **249**, 386 (1990); J. J. Devlin, L. C. Panganiban, P. E. Devlin, *ibid.*, p. 404; S. E. Cwirla, E. A. Peters, R. W. Barrett, W. J. Dower, *Proc. Natl. Acad. Sci. U.S.A.* **87**, 6378 (1990); C. F. Barbas, A. Kang, R. A. Lerner, S. J. Benkovic, *ibid.* **88**, 7978 (1991); C. Tuerk and L. Gold, *Science* **249**, 505 (1990); A. D. Ellington and J. W. Szostak, *Nature* **346**, 818 (1990); A. M. Bray, N. J. Maeji, H. M. Geysen, *Tetrahedron Lett.* **31**, 5811 (1990); R. A. Houghten *et al.*, *Nature* **354**, 84 (1991); K. S. Lam *et al.*, *ibid.*, p. 82; J. Blake and L. Litzi-Davis, *Bioconjugate Chem.* **3**, 510 (1992); M. C. Needels *et al.*, *Proc. Natl. Acad. Sci. U.S.A.* **90**, 10700 (1993); M. H. J. Ohlmeyer *et al.*, *ibid.*, p. 10922.
6. S. P. A. Fodor *et al.*, *Science* **251**, 767 (1991).
7. B. A. Bunin, M. J. Plunkett, J. A. Ellman, *Proc. Natl. Acad. Sci. U.S.A.* **91**, 4708 (1994).
8. Sputtering was carried out at 10^{-5} to 10^{-6} torr, with Ar as the sputtering gas; deposition rates were 0.1 to 1 Å s^{-1}. Film thickness was monitored with a crystal microbalance and calibrated independently with a profilometer. The uniformity of the deposited films varied less than 5% over an area 2 inches in diameter.
9. The library was generated using the following deposition sequence (deposition step, element, secondary mask number): 1, Bi, M1; 2, Pb, M2; 3, Cu, M0 (no mask); 4, Ca, M3; 5, Sr, M4.
10. Seemann-Bohlin x-ray diffraction measurements were carried out with thin films (5 mm by 5 mm) deposited and sintered along with libraries under the conditions described above. The films are generally not highly oriented, and no effort has yet been made to correlate transport properties with x-ray structures.
11. A. W. Sleight, *Science* **242**, 1519 (1988); R. J. Cava, *ibid.* **247**, 656 (1990); H. Maeda *et al.*, *Jpn. J. Appl. Phys.* **27**, L209 (1988) and references therein.
12. L. Fister, T. Novet, C. A. Grant, D. C. Johnson, *Adv. Synth. React. Solids* **2**, 155 (1994).
13. Samples were generated by sequential deposition of Bi_2O_3, $SrCO_3$, CaO, and CuO in a molar ratio of 2:2:2:3 with a Bi_2O_3 film thickness of 500 Å. Samples were sintered at 840°C in air.
14. See, for example, S. Jin *et al.*, *Science* **264**, 413 (1994).
15. G. Briceño *et al.*, Abstracts of the American Physical Society Meeting, March 1995, A24.

16. Supported by the Laboratory Directed Research and Development Program of Lawrence Berkeley Laboratory under the U.S. Department of Energy, contract DE-AC03-76SF00098, and the Office of Naval Research, grant N00014-93-1-0380. G.B. acknowledges support from a UC President's postdoctoral fellowship. We thank Symyx Technologies (Menlo Park, CA), I. Goldwasser, J. Torrance, and E. Granlund for helpful advice.

7 December 1994; accepted 24 March 1995

Hubble Space Telescope Imaging of Neptune's Cloud Structure in 1994

H. B. Hammel,* G. W. Lockwood, J. R. Mills, C. D. Barnet

Images of Neptune taken at six wavelengths with the Hubble Space Telescope in October and November 1994 revealed several atmospheric features not present at the time of the Voyager spacecraft encounter in 1989. Furthermore, the largest feature seen in 1989, the Great Dark Spot, was gone. A dark spot of comparable size had appeared in the northern hemisphere, accompanied by discrete bright features at methane-band wavelengths. At visible wavelengths, Neptune's banded structure appeared similar to that seen in 1989.

In 1989, the Voyager 2 spacecraft flew by the planet Neptune, revealing remarkable atmospheric activity on the most distant giant planet (*1*). Blue wavelength images were dominated by a single large storm in the southern hemisphere [see, for example, figure 8 in (*1*)]; the feature, dubbed the "Great Dark Spot" (hereafter, GDS-89) because of its prominence, was tracked for months (*2*). However, despite its size, the feature's low contrast put it beyond the reach of subsequent ground-based or Hubble Space Telescope (HST) imaging until HST's 1993 refurbishment. Thus, the feature's long-term survival was the subject of speculation (*3*). Meanwhile, ground-based near-infrared images suggested dramatic changes in Neptune's large-scale atmospheric features: activity appeared to be shifting from the southern hemisphere to the northern hemisphere (*4*). Moreover, the overall brightness of the planet increased by several percent, continuing a long-term trend (*5*), and initial imaging with the repaired HST hinted that GDS-89 might have disappeared, although the time sampling of the observations was insufficient to make a definitive statement (*6*).

In late 1994, we obtained multiwavelength images of Neptune with HST. The images show that the planet's appearance has indeed changed dramatically since 1989: we confirm that GDS-89 is gone and report a new dark feature of comparable size in the northern hemisphere, most clearly visible in blue light (Figs. 1 and 2). At methane-band wavelengths, the planet's appearance is dominated by several large, rapidly changing features at northern mid-latitudes, including clouds clearly associated with the new dark spot. Each set of images, taken a few hours apart, was timed to ensure nearly complete longitudinal coverage on three separate HST visits: 10 to 11 October 1994, a week later on 18 to 19 October 1994, and finally, 3 weeks later on 1 to 2 November 1994 (Table 1).

Neptune's disk (diameter, 2.2 arc sec) extended over 48 pixels on HST's Planetary Camera. One pixel corresponded to 990 km at disk center, about six times better than the resolution in excellent ground-based images. We used the standard image calibration and processing provided by the Space

H. B. Hammel and J. R. Mills, Department of Earth, Atmospheric, and Planetary Sciences, Massachusetts Institute of Technology, Cambridge, MA 02139, USA.
G. W. Lockwood, Lowell Observatory, Flagstaff, AZ 86001, USA.
C. D. Barnet, Space Astrophysics Laboratory, Institute for Space and Terrestrial Science, North York, Ontario M3J 3K1, Canada.

*To whom correspondence should be addressed.

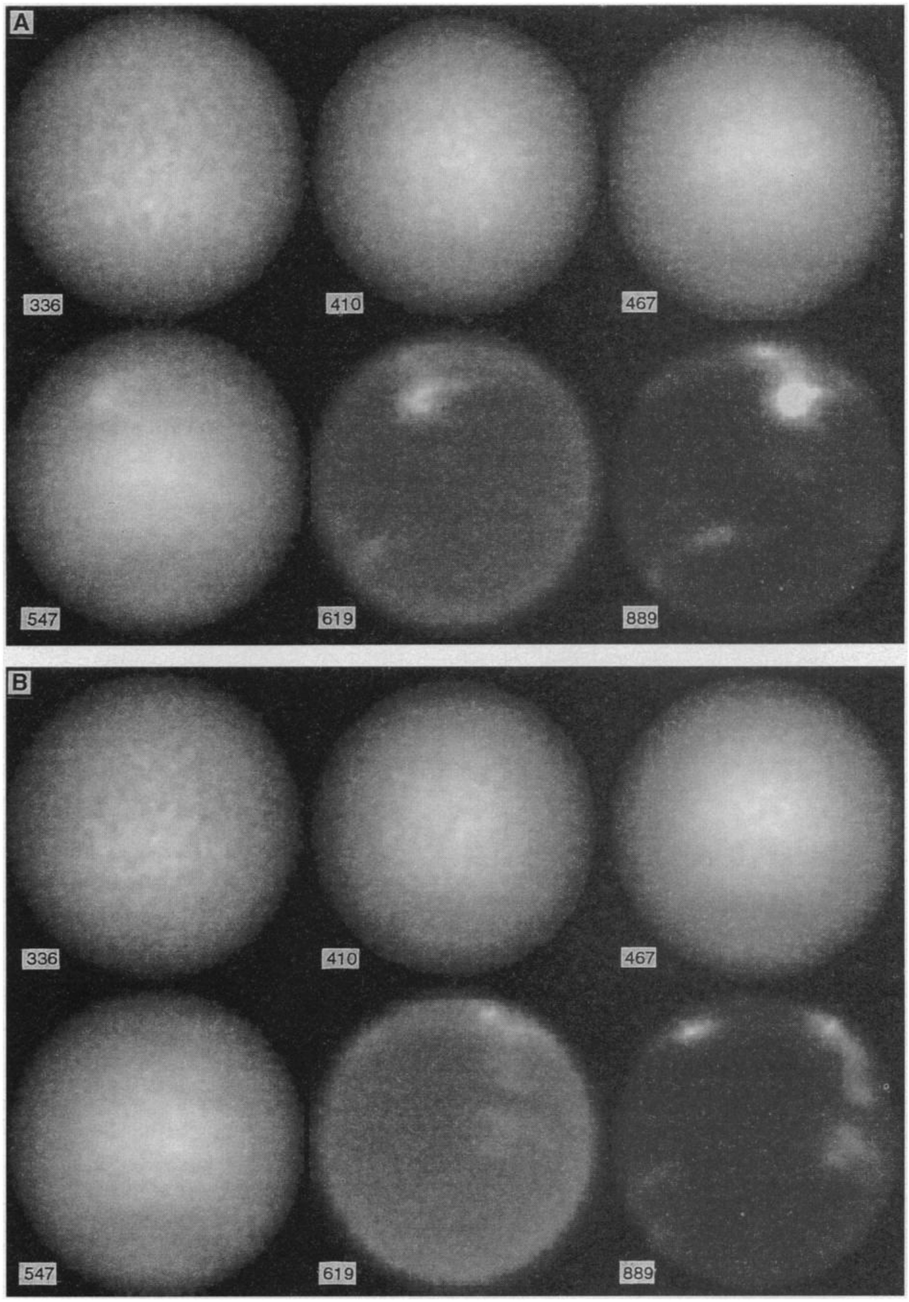

Fig. 1. Temporal variability of Neptune's cloud structure. The wavelengths (indicated at bottom left of each image) are (top row) 336, 410, and 467 nm (ultraviolet, far blue, and blue) and (bottom row) 547, 619, and 889 nm (green, red, and near-infrared). The 619- and 889-nm methane-band images are strongly limb-brightened as a result of stratospheric aerosols; they are enhanced with a logarithmic stretch. The dark band from −55° to about −70° was seen in Voyager images, as was the south polar brightening in the 619-nm images (*1*). North is up, Neptune west longitude increases to the left (planetary rotation is evident), and the sub-Earth latitude is −25°. (**A**) Images obtained on 10 October 1994. A new Great Dark Spot (GDS-94) is initially located on the extreme upper left in the images in the top row, although the dark feature itself is only easily seen in map projections. The complex of bright features associated with GDS-94 is detectable even at visible wavelengths and dominates methane-band images. Other clouds are visible, including discrete features at −30° and −45°. (**B**) Images obtained on 2 November 1994. GDS-94 can be seen in the visible-wavelength images as a dark streak near Neptune's northern limb; its shape is distorted as a result of extreme projection (see Fig. 2). The bright complex has faded at all wavelengths and is no longer detectable at 547 nm. Although differential rotation caused a relative shift between the complex and the features at −30° and −45°, the complex itself did not shear; it may be a standing wave pattern associated with GDS-94 (*9*).

Telescope Science Institute (*7*). We then converted from pixel coordinates to planetographic latitudes and west longitude (*8*).

At visible wavelengths, we detected dark bands (Fig. 1): a strong one extending from a latitude of −55° to about −68°, and a weaker one near −32°, the same latitudes where dark bands occurred in Voyager images (*1*). At blue wavelengths, there was no feature in Neptune's southern hemisphere resembling GDS-89. That feature would have subtended roughly 6 pixels by 16 pixels and was darker than the −60° band seen in our HST images. We have complete longitudinal coverage of its −22° latitude in each of our three visits; it should have been easily seen. If the feature still exists, it has either shrunk by

Table 1. Observation log for images presented here.

10 October 1994		2 November 1994		Filter		Exposure
UT time	CML*	UT time	CML*	Name	λ (δλ) (nm)†	(s)
20:26:16	285.0	05:56:16	54.7	F336W	332.14 (37.97)	140
20:31:16	286.8	06:01:16	56.6	F410M	409.04 (14.65)	70
20:35:16	288.3	06:05:16	58.0	F467M	466.86 (16.63)	50
20:39:16	289.8	06:09:16	59.5	F547M	547.79 (48.61)	14
20:54:16	295.4	06:25:16	65.5	FQCH4N15	620.82 (3.96)	350
22:14:16‡	325.2	07:37:17‡	92.3	FQCH4P15	888.45 (14.63)	700

*Central meridian longitude of image (*8*). †λ and δλ are the central wavelength and bandpass from table 6.2 of (*15*). F467M was chosen to match the wavelength of greatest contrast of GDS-89 in Voyager images (*1*). The F467M and F547M wavelengths closely match those used for the long-term disk-integrated brightness monitoring (*5*); FQCH4N15 matches the Voyager MeJ methane filter, and FQCH4P15 matches a filter used for a long-term ground-based imaging program (*16*). N15 and P15 indicate positions of the partially rotated filter wheel (*15*). ‡The first five images were obtained in one HST orbit; the 889-nm images were obtained in the next orbit.

more than a factor of 4 or its contrast has been reduced by more than a factor of 2, or both. Furthermore, the "Bright Companion" to GDS-89 was no longer seen after 1992 (*4*), also indicative that GDS-89 was no longer a dominant feature.

We detected a new large dark spot on Neptune at +30° (hereafter, GDS-94). Although it was very close to the northern limb, it was visible in reprojected maps from the first and third visits (Fig. 2); we did not sample its longitude on the second visit. The size of GDS-94, 13° in latitude and 35° in longitude, is similar to that of GDS-89, 15° by 38° (*1*). The new feature had a rotation period of 18.4 hours, consistent with the zonal wind profile determined from Voyager data (*2*). Although GDS-89 was last seen heading northward in mid-1989 at a rate of roughly 1° per month (*2*), it is unlikely that that storm survived traversal of Neptune's equatorial region: the reversal of the zonal wind pattern would probably have rendered the vortex unstable and caused its disruption (*9, 10*). At a wavelength of 467 nm, GDS-94 has contrast of about −0.05 (*11*), compared with the Voyager 480-nm contrast of about −0.1 for GDS-89 (*1*).

At methane-band wavelengths, 619 and 889 nm, the planet has several large, high-contrast features near +27° latitude, a region of activity in Voyager images (*1*). Some are bright enough to be seen at continuum (nonmethane) wavelengths. Most interesting is a complex of features associated with GDS-94 (Fig. 1): a bright feature just a few degrees north of GDS-94 and other bright components extending 30° southward to nearly the equator. If these features moved with the local zonal winds, the pattern should have sheared over 3 weeks as a result of differential rotation (*2*). However, in all three visits, the components of the complex retained their relative shapes and proximity.

GDS-89 had a remarkably similar stable configuration extending over a comparable latitude range, but its pattern was inverted in latitude as compared with that of GDS-94; GDS-89 had a bright companion feature just southward and an accompanying bright "ghost" feature northward near the equator (+3°) that retained its relative position for at least a month (*1*). Models of Neptune atmospheric dynamics suggest that a GDS may create such stable structures by generating a standing wave pattern that may affect temperatures and pressures many degrees away from the vortex itself (9). The companion clouds' visibility in the 889-nm methane band (both for GDS-89 and GDS-94) suggests that they are relatively high in altitude (*12*).

Reports of cloud features on Neptune date from the visual observations by Dollfus in 1948 (*13*), although such sightings were rare and difficult because of Neptune's tiny disk and low altitude for observers in the Northern Hemisphere. On the other hand, multiple bright clouds in one hemisphere or the other (and sometimes both) are ubiquitous in modern digital images at near-infrared methane-band wavelengths, where their contrast is maximized (*14*). Because both of the large dark features discovered to date have been associated with bright methane-band features, one is tempted to infer that past bright features indicated the presence of similar GDSs.

In summary, two observing intervals 5 years apart show little evidence of permanent discrete cloud features on Neptune, although the pattern of low-contrast banding seems more stable, like similar bands on Jupiter and Saturn. Cloud structures, some quite large, come and go; the largest detected in 1994 appear at a latitudinal band where only hints of activity were seen in 1989. The disappearance of GDS-89 indicates limited temporal existence for such features; the detection of GDS-94 now provides an opportunity to determine a feature's actual lifetime by continuing HST observations of this active planetary atmosphere.

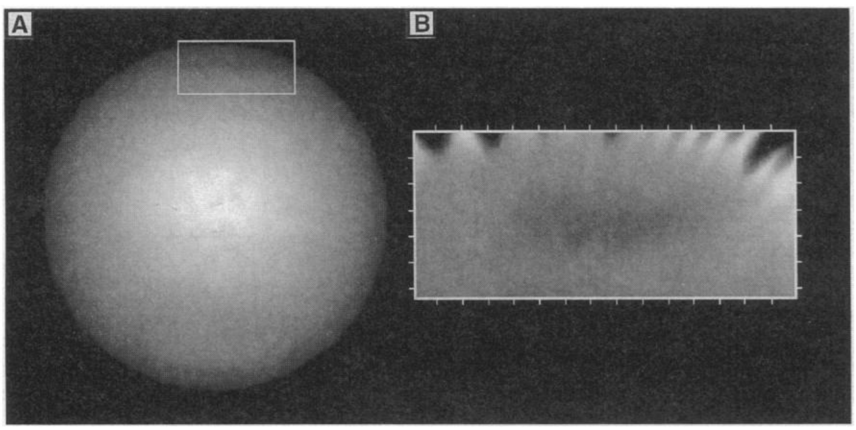

Fig. 2. Neptune's new dark feature. (**A**) An HST image of Neptune taken at 467 nm on 2 November 1994. The Great Dark Spot discovered by Voyager (GDS-89) had maximum contrast at this wavelength and was located at a latitude of about −22° (*1*). There is no evidence for GDS-89 in this or any other 467-nm HST image. Orientation is the same as Fig. 1. (**B**) A rectilinear map of the dark streak close to the northern limb of the image in (A). When the geometric projection effect is removed, the feature is revealed as a large dark oval (*8*). This feature (GDS-94) is comparable in size and shape to GDS-89; tick marks are 5° in both latitude and longitude. GDS-94 is probably a new feature: the zonal winds reverse direction in the northern hemisphere, and thus, GDS-89 probably fell apart if it approached the equator. Distortions near the northern limb are an artifact of the reprojection.

REFERENCES AND NOTES

1. B. A. Smith *et al.*, *Science* **246**, 1422 (1989).
2. H. B. Hammel *et al.*, *ibid.* **245**, 1367 (1989); S. S. Limaye and L. A. Sromovsky, *J. Geophys. Res.* **96**, 18941 (1991); L. A. Sromovsky, S. S. Limaye, P. M. Fry, *Icarus* **105**, 110 (1993).
3. During the 1989 Voyager encounter, GDS-89 exhibited changes in size and shape (*1*) and drifted in both latitude and longitude (*2*). In contrast, Jupiter's largest atmospheric storm, the Great Red Spot, has been constant in size, shape, and location for over 100 years [R. F. Beebe *et al.*, *NASA SP-494* (National Aeronautics and Space Administration, Washington, DC, 1989), p. 245].
4. H. B. Hammel, paper presented at the 25th Annual Division of Planetary Sciences Meeting, Boulder, CO, 18 to 22 October 1993.
5. G. W. Lockwood and D. T. Thompson, *Nature* **349**, 593 (1991).
6. D. Crisp *et al.*, *Bull. Am. Astron. Soc.* **26**, 1093 (1994).
7. J. A. Biretta *et al.*, in *Calibrating Hubble Space Telescope*, J. C. Blades and S. J. Osmer, Eds. (Space Telescope Science Institute, Baltimore, MD, 1993), p. 8.
8. We used the 1991 pole position [M. E. Davies *et al.*, *Celestial Mech. Dyn. Astron.* **53**, 377 (1992)] and the 16.11-hour radio rotation period [J. W. Warwick *et al.*, *Science* **246**, 1498 (1989)]. Navigation, coordinate transformations, and map reprojection were performed with the programs SALNAV and AMIE, which were originally developed for Voyager data reduction and were subsequently modified by C. D. Barnet and D. DelRizzo.
9. R.-P. LeBeau and T. E. Dowling, personal communication.
10. This view is supported by theoretical studies of vortices on Jupiter [T. E. Dowling and A. P. Ingersoll, *J. Atmos. Sci.* **46**, 3256 (1989); G. P. Williams and R. J. Wilson, *ibid.* **45**, 207 (1988); P. S. Marcus, *Nature* **331**, 693 (1988)] and actual observations of jovian vortices [M.-M. Mac Low and A. P. Ingersoll, *Icarus* **65**, 353 (1986)].
11. Contrast is defined as $(I_f/I_b - 1)$, where I_f and I_b are the brightnesses of the feature and the surrounding background.
12. H. B. Hammel, K. H. Baines, J. T. Bergstralh, *Icarus* **80**, 416 (1989); K. H. Baines and H. B. Hammel, *ibid.* **109**, 20 (1993).
13. B. Lyot, *L'Astronomie* **6**, 3 (1953).
14. B. A. Smith, H. J. Reitsema, S. M. Larson, *Bull. Am. Astron. Soc.* **11**, 570 (1979); H. B. Hammel, *Icarus* **80**, 14 (1989).
15. C. J. Burrows, Ed., *Wide Field and Planetary Camera 2 Instrument Handbook* (Space Telescope Science Institute, Baltimore, MD, May 1994).
16. H. B. Hammel *et al.*, *Icarus* **99**, 363 (1992).

17. We thank E. Holmes for data analysis, acknowledge the Wide Field and Planetary Camera 2 (WFPC2) team for the excellent instrument, and appreciate the assistance of the staff at Space Telescope Science Institute (STScI). These National Aeronautics and Space Administration (NASA) and European Space Agency HST observations were supported by grant GO-5329.01-93A from STScI, which is operated by the Association of Universities for Research in Astronomy under NASA contract NAS5-26555.

13 February 1995; accepted 18 April 1995